Evaporation of a single ethanol droplet interacting with a premixed laminar CH_4/air flame

Deniz Kaya*[1,2,3], Guillaume Renoux[1,2], Fabien Halter[1,2], Ahmet Yozgatlıgil[3],
İskender Gökalp[1,3], Christian Chauveau[1]
[1]CNRS-INSIS, Institut de Combustion, Aérothermique, Réactivité et Environnement, Orléans, France
[2]Université d'Orléans, Orléans, France
[3] Department of Mechanical Engineering, Middle East Technical University, Ankara, Turkey
*Corresponding author email : deniz.kaya@cnrs-orleans.fr

Abstract
Among all phenomena occurring in liquid-fueled combustion chambers, one basic process is the interaction of droplets with the flame. Therefore, it is essential to understand the dynamics of an individual droplet interaction with a flame front in order to analyze more complex flames.
The aim of this study is to investigate the evaporation of a single ethanol droplet interacting with a premixed laminar CH_4/air flame. In the experimental part of the study, the droplet was injected into the stagnation flame. The visualization of the flame front and the temporal monitoring of the droplet evaporation were performed using optical technics (PIV, PTV, ILIDS). In the numerical part of the study, single droplet evaporation under constant temperature and stagnant environment was studied with the Eulerian-Lagrangian approach using the YALES2 solver. The variations of the droplet and gas properties were computed under N_2 atmosphere and under flame conditions. From the vaporization rate calculations, it is observed that there is a slight effect of flame stretch due to the change in the temperature profile. It is also observed that the flame temperature has a dominant effect on the evaporation rate rather than the burnt gas composition.

Keywords
Two-phase combustion, droplet evaporation, stagnation flame, Spalding model.

Introduction

In order to obtain high energy efficiency in spray combustion applications, high rates of evaporation and rapid mixing of liquid fuel with the gas phase are desired. The vaporization characteristics and the initial properties of the droplet may also affect the flame structure. Therefore, a detailed analysis of vaporization and burning rates of droplets is required.
Ethanol is an extensively studied fuel as an oxygenated additive and it can be produced from bio-based processes. Many studies report the evaporation of pure ethanol and its mixtures under several conditions from both experimental and numerical aspects [1–4]. However, there are still many points to be clarified in terms of change in vaporization characteristics due to the presence of the flame and the dependency of vaporization rate on several parameters.
In this study, the evaporation of an isolated single ethanol droplet interacting with a laminar premixed CH_4/air flame is studied experimentally and numerically. The evaporation rate of the droplet is measured under different flame conditions and its dependency to the droplet initial diameter and gas temperature profile are investigated. The simulations are performed with the Spalding model under stagnant N_2 atmosphere and burnt gas conditions at constant temperature and compared with the experimental results.

Experimental Methods

A flat flame burner is used in order to observe the droplet evaporation sequence through a stationary laminar flame. The mixture of air and CH_4 is supplied to the burner by a seeding system with N_2 co-flow in order to facilitate flame stabilization. The flame can be stabilized nearly 10 mm upstream to the burner outlet thanks to the presence of an upper stagnation plate. The monodispersed liquid ethanol droplets with 50 μm diameter are fed to the system perpendicularly by an injector. The schematic of flat flame burner and the laminar flame image are given in Figure 1. The burner is coupled with two high-speed cameras and a laser device emitting at 532 nm to create a 2D laser sheet in the presence of di-ethylhexyl-sebacate (DEHS) droplets.

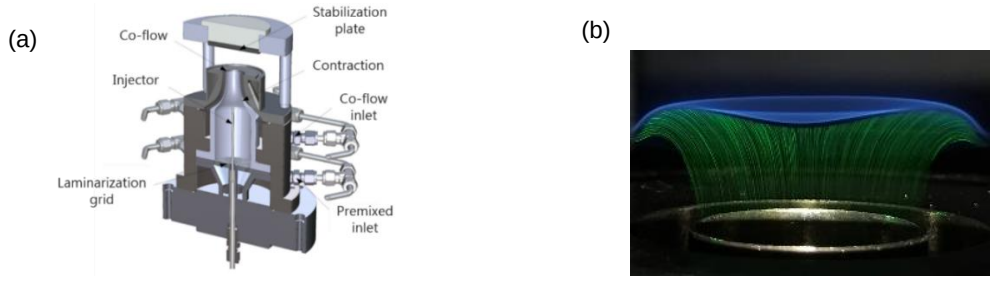

Figure 1. (a) Schematic of the flat flame burner [5] (b) Image of the laminar CH_4/air flame with DEHS droplets illuminated by a 2D laser sheet

Visualization of the flame front and temporal monitoring of the droplet evaporation are performed using planar laser tomography. Mie scattering is utilized to determine the position of the flame front and the velocity of unburnt gases via Particle Image Velocimetry (PIV). The location of the flame front is determined at T=525 K where DEHS droplets evaporate. In order to measure the velocity of unburnt gases, an open-source MATLAB library PIVlab is used [6]. The motion of the droplet is also determined via Mie scattering using Particle Tracking Velocimetry (PTV). For each frame, the location of the ethanol droplet is tracked with Kanade-Lucas-Tomasi (KLT) feature tracking algorithm in MATLAB Computer Vision library and the velocity of the droplet is calculated.

In addition, Interferometric Laser Imaging for Droplet Sizing (ILIDS) is coupled with Mie scattering in order to obtain the droplet size variation during evaporation. The high-speed camera for ILIDS allows obtaining a good temporal resolution for the evolution of the droplet size by defocusing and capturing the interference fringe pattern of the droplet at each frame. The number of fringes is computed for an individual droplet at each frame based on Discrete Fourier Transform (DFT) on the five vertical sections of the fringe pattern. With the help of peak intensities in Fourier space, the fringes are detected and computed. The droplet diameter based on the number of fringes is then calculated; 3.52 μm/fringe resolution is obtained in this configuration [7].

The cameras for PIV/PTV and ILIDS have different acquisition frequencies, 40,000 and 10,000 images per second, respectively. They are synchronized in time in order to combine the different diagnostics. Experiments are performed with ethanol droplet and CH_4/air premixed flame at equivalence ratios of 0.8, 0.9, 1.0 and 1.1 calculated only considering CH_4 as fuel, since the quantity of ethanol added is negligible compared to the CH_4 flow rate. For each sequence, individual droplets are selected over all recordings and the complete postprocessing is performed for the droplet.

Computational Methods

Laminar flame computations are performed with Cantera [8] using COFFEE mechanism with 14 species and 39 reactions [9] and detailed San Diego mechanism with 57 species and 268 reactions [10]. Adiabatic 1D freely propagating and stagnation flame configurations are computed at ϕ=0.8, 0.9, 1.0 and 1.1 for CH_4/air premixed flames in order to differentiate the effect of stretch on evaporation. From PIV results, the position of the flame front is determined based on the presence of DEHS droplets. By taking the isotherm T=525 K as the evaporation temperature, calculated temperature profiles, thermodynamic and transport properties are fitted to the experimental flame field in order to track the droplet evaporation through the flame field.

Evaporation simulations are performed with YALES2 solver based on the finite volume method for low Mach number flows with variable density [11]. Eulerian-Lagrangian (EL) approach is used to model the two-phase flow in which a droplet is considered as an isolated point in Lagrangian frame, while the gas phase is represented with the Eulerian description.

The evaporation of the droplet is modelled using Spalding model [12]. Droplets are assumed to be spherical, isolated, mono-component, having infinite thermal conductivity and uniform temperature. The surface of the droplet is assumed to be in thermodynamic equilibrium with the surrounding gas and the Clausius-Clapeyron relation is used to calculate the partial saturated vapor pressure of ethanol at the surface of the droplet:

$$P_{surf} = P_{ref}\, exp\left[\frac{W\, L_v}{R}\left(\frac{1}{T_{evap}} - \frac{1}{T_p}\right)\right] \tag{1}$$

For the integration of the evaporation model, the droplet mass temporal evolution is determined assuming the fuel mass flux leaving the droplet surface equal to the variation of mass of a droplet:

$$\frac{dm_p}{dt} = \pi\, d_p\, Sh\, \rho_p\, \mathcal{D}\, log(1 + B_M) \qquad B_M = \frac{Y_{surf} - Y_\infty}{1 - Y_{surf}} \tag{2}$$

The temperature and species mass fractions at the far field are computed with the 1/3 rule. Using the relation for mass variation proposed by Spalding, droplet diameter variation is expressed as:

$$d_p^{\,2} = d_{p,0}^{\,2} - \frac{8\rho_g D}{\rho_p} ln(B_M + 1)\, t \tag{3}$$

The temporal evolution of the droplet temperature is estimated by integrating the energy conservation equation from the surface of the droplet to the far field:

$$\frac{dT_p}{dt} = \frac{1}{\tau_h}\left[T_p - \left(T_\infty - \frac{L_v\, B_T}{C_{p,ref}}\right)\right] \qquad B_T = (1 - B_M)^{\beta} - 1 \qquad \beta = \frac{Sh\, Pr}{Nu\, Sc} \tag{4}$$

Sh and Nu numbers are computed without a convective correction and with the particle Reynolds number based on particle velocity measured at gas reference frame. Pr and Sc numbers are calculated by assuming that the surface of the droplet is in thermodynamic equilibrium with the surrounding gas.

For computations, an isolated ethanol droplet is injected at T=300 K and P=1 atm at the center of a large Cartesian cube with dimensions 10×10×10 cm^3 to avoid edge effects. The evaporation of the droplet is tracked until complete evaporation at constant temperature and stagnant ambient with pure N_2 and burnt gases. Burnt gas compositions are computed in Cantera for equivalence ratios ranging between 0.8-1.1 with different kinetic mechanisms.

Droplet diameter, droplet temperature, Spalding numbers and gas properties are computed during evaporation process.

Results and Discussion

Since Rayleigh scattering signal is completely shadowed by the Mie scattering signal, the temperature of the gas field cannot be obtained experimentally during PIV/PTV measurements. Instead, the temperature profiles for 1D adiabatic freely propagating and stagnation premixed CH_4/air flames with COFFEE scheme are computed in Cantera at different equivalence ratios and the computed profile is fitted to the experimental field. In Figure 2.a, fitted stagnation temperature profile and the ethanol droplet trajectory during the evaporation process are given. In Figure 2.b, the droplet diameter evolution under different temperature profiles are reported for the same case. It is seen that there is a slight change in the temperature profile after the reaction zone due to the stretch.

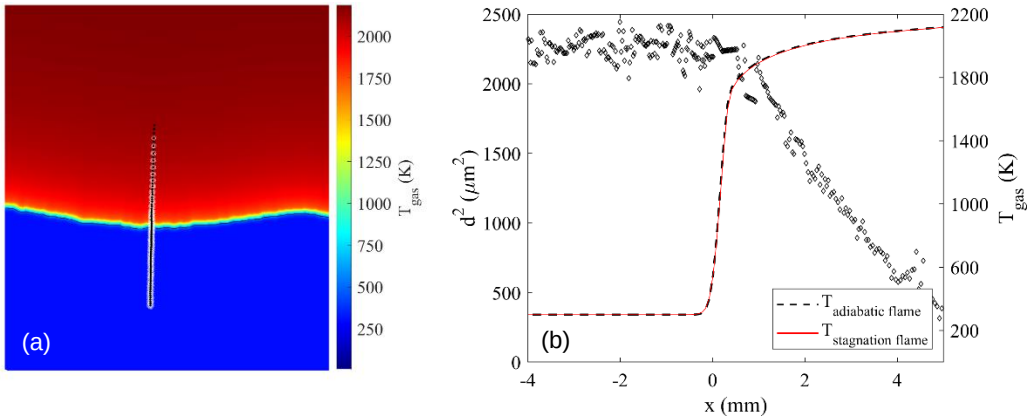

Figure 2. (a) Fitted stagnation temperature profile and droplet trajectory (b) Variations in the droplet diameter and gas temperature for a stabilized stoichiometric CH_4/air flame and ethanol droplet (d_0 = 45 μm)

In order to compute the droplet evaporation rate, K, slope of d^2 vs t is computed over the diameter change interval. For each droplet, the mean temperature in this interval is recorded with the minimum and maximum values. Although the K values are in an acceptable range for all droplets having the same equivalence ratio, there are slight changes due to the difference in the initial position of the captured droplet and the droplet diameter measurement quality at certain frames. Since individual droplets are selected over all recorded experimental data, some droplets are initially tracked closer to the flame front. Therefore, the measured droplet trajectory is shorter for these droplets, making them difficult to track. Also, there may be some local deviations with a small error on the computed droplet diameter, especially close to the flame region where the change in diameter is expected to be higher in a shorter distance due to the steep temperature profile.

Figure 3 shows the dependency of the evaporation constant to the initial droplet size. Mean K values are computed and reported over all samples at each equivalence ratio, with the error bars. For stoichiometric and rich flame conditions, large error bars are observed. However, it can be clearly seen that the majority of K values are located around 0.59 and 0.65 mm^2/s for φ=1.1 and 1.0, respectively. For lean flame conditions, it is seen that the variation range of K is even smaller. Therefore, it can be concluded that there is no major dependency of the evaporation constant to the initial size of the droplet. Nevertheless, small deviations can be observed due to different experimental conditions and the initial position of

the droplet affecting the time spent at a certain temperature interval. It is also known that the vaporization rate of large droplets may be affected by drag forces.

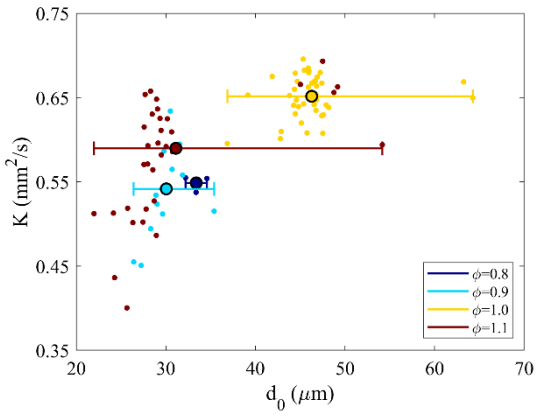

Figure 3. Changes in ethanol evaporation constant with respect to the initial droplet diameter at different equivalence ratios

The comparison between experimental and numerical ethanol droplet evaporation rates is performed under stagnant N_2 ambience conditions. Saharin et al. studied the evaporation of isolated, anhydrous ethanol droplets [13]. The experiments were performed under N_2 ambience at varying temperatures between 373-673 K and the temporal evolution of the droplet diameter was recorded using a high-speed camera. The results are given in Figure 4, with the numerical results for corresponding cases.

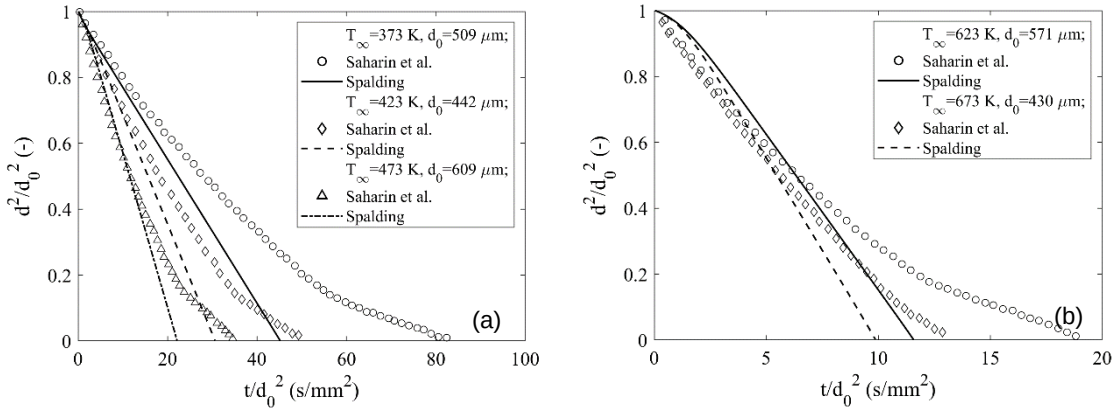

Figure 4. Comparison of the ethanol droplet evaporation computations with the experiments of Saharin et al. [13] Spalding model under pure N_2 ambience at P=1 atm (a) low temperature (b) high temperature

Saharin et al. observed a deviation from the linear evaporation profile due to the condensation of water vapor on the droplet surface and the simultaneous evaporation of ethanol and water. The condensation effect is observed to be more important at lower ambient temperatures because of the high miscibility of ethanol to water. However, for high temperature cases, a linear behaviour is observed for ethanol evaporation with a higher droplet lifetime than the one computed with the Spalding model. Due to the experimental technique used in the measurements, it is expected to observe a lower evaporation constant since the droplet conserve its sphericity and the effects of heat conduction in the quartz fiber are limited; leading to the observation of higher evaporation times [14]. Noting that Pr and Sc

numbers are constant in the Spalding model, the numerical results are still in good agreement with the experiments, especially at higher ambient temperatures.

In order to compare the numerical results with flame experiments, burnt gas compositions are calculated in Cantera. COFFEE and San Diego mechanisms are used to differentiate the effect of species available in the surrounding gas since the latter contains ethanol in gas phase reactions. Evaporation computations are performed for each equivalence ratio at the ambient temperature varying between 1800-2200 K and at the burnt gas compositions, as well as at the flame compositions. It is observed that for lean and rich flame conditions, the evaporation constant is almost the same with the two mechanisms due to the fact that the compositions of major species are almost the same and the composition of ethanol is nearly negligible. For stoichiometric flame condition, the difference between the evaporation constants at lower ambient temperature (1800-1900 K) is ~0.02 mm^2/s which is decreasing towards higher temperatures. It is clearly seen that the ambient gas composition has no major effect on the evaporation under evaluated conditions.

In Figure 5, evaporation constants are plotted against the gas temperature for experimental and numerical cases. For the Spalding model results at the burnt gas conditions, only one case is included for the sake of clarity since the computed evaporation constant is almost the same at different equivalence ratios with both kinetic mechanisms.

It is observed from the experiments that K values are varying between 0.6-0.7 mm^2/s for the stoichiometric flame while for ϕ=0.9 and 1.1, a wider range is observed. It should be noted that this is mostly due to the high sampling at these equivalence ratios and aforementioned reasons. Hence, instead of selecting some droplets, the mean values of K, mean interval temperature, minima and maxima are computed and reported in Figure 5 over all samples at each equivalence ratio based on the stagnation flame temperature profile.

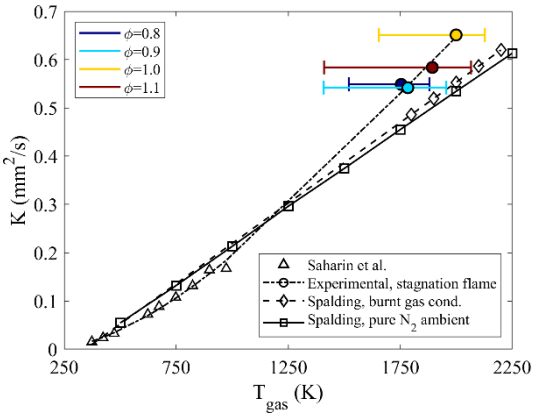

Figure 5. Comparison of ethanol evaporation constant with respect to temperature

It is observed that the Spalding model overestimates the evaporation rate for low temperatures when it is compared with the experimental results of Saharin et al. However, for high temperatures and flame conditions, higher evaporation rates are measured experimentally. It should also be noted that Re_p numbers are computed for all cases as ~0.1 in order of magnitude indicating that there is no major effect of relative velocity for the droplet.

The evaporation temperature is selected as the mean temperature in an interval where the droplet starts evaporating and its lifetime ends, since there is no way to measure the exact evaporation temperature of a moving droplet through a flame field. Still, maxima of the measured evaporation constants are very close to the numerical results. Although, there is a

slight difference due to the different temperature profiles of the two flame configurations. From the comparison of adiabatic flame and stagnation flame temperature profiles, it is observed that same K values yield lower mean interval temperatures for stagnation flames with a wider range from the minimum value. In other words, the droplet starts to evaporate at lower temperatures through the stagnation flame and the lifetime of the droplets ends at comparably similar temperatures for both flames. From these results, it can be interpreted that the flame stretch has an impact on evaporation by lowering the ambient temperature which the droplet is exposed to while evaporating.

Conclusions

Evaporation of a single ethanol droplet under flame conditions is studied. Experiments are conducted in a stagnation flame burner configuration where the droplet is injected through a laminar, flat and stationary premixed CH_4/air flames at ϕ=0.8, 0.9, 1.0 and 1.1. The diameter of the droplet is measured via ILIDS at each frame and the evaporation rate is calculated by fitting a temperature profile computed from Cantera for 1D adiabatic freely propagating and stagnation flame configurations. It is observed that the droplet is exposed to higher temperatures for an adiabatic flame configuration due to the differences in temperature profiles. The major cause of this phenomenon is the flame stretch. Hence, the presence of stretch affects the evaporation rate of the droplet slightly. It is also observed that the initial diameter of the droplet has no major effect on the evaporation rate. Numerical computations are performed under pure N_2 ambient and burnt gas compositions for an isolated ethanol droplet. While pure N_2 ambience computations agree well with the literature at low temperatures, Spalding model underestimates the evaporation rate at higher temperatures. It is also concluded that ethanol droplet evaporation under the present conditions is not directly affected by the changes in ambient gas composition at flame conditions.

Acknowledgments

The authors would like to acknowledge CNRS CORIA for permitting the use of YALES2 code and express special thanks to Dr. Vincent Moureau for his guidance. DK acknowledges the financial support of the French Embassy in Ankara for her joint PhD program between METU and the Université d'Orléans and TÜBİTAK BİDEB 2211-C scholarship programme.

Nomenclature

ρ_g	density of the gas phase [kg/m^3]
ρ_p	density of the droplet [kg/m^3]
$\mathcal{D}$	thermal diffusivity [m^2/s]
τ_h	thermal characteristic time [s]
B_M	Spalding mass number [-]
B_T	Spalding heat number [-]
$C_{p,ref}$	reference heat capacity [J/K]
d_p	diameter of the droplet [m]
$d_{p,0}$	initial diameter of the droplet [m]
K	evaporation rate [m^2/s]
L_v	latent heat of vaporization [J/kg]
m_p	mass of the droplet [kg]
Nu	Nusselt number [-]
P_{ref}	reference pressure [Pa]
P_{surf}	surface pressure [Pa]

Pr Prandtl number [-]
R universal gas constant [= 8.314 J/mol K]
Re_p Reynolds number of the droplet [-]
Sc Schmidt number [-]
Sh Sherwood number [-]
t time [s]
T_{evap} evaporation temperature [K]
T_p temperature of the droplet [K]
T_{ref} reference temperature [K]
T_∞ temperature of the gas phase [K]
W molar mass [kg/mol]
Y_{surf} evaporated mass fractions at the surface of the droplet [-]
Y_∞ evaporated mass fractions of the gas phase [-]

References

[1] Muelas, Á., Carpio, J., Ballester, J., Sánchez, A. L., and Williams, F. A., 2020, "Pyrolysis Effects during High-Temperature Vaporization of Alkane Droplets," Combustion and Flame, 217, pp. 38–47.
[2] Millán-Merino, A., Fernández-Tarrazo, E., and Sánchez-Sanz, M., 2021, "Theoretical and Numerical Analysis of the Evaporation of Mono- and Multicomponent Single Fuel Droplets," Journal of Fluid Mechanics, 910.
[3] Pinheiro, A. P., Vedovoto, J. M., da Silveira Neto, A., and van Wachem, B. G. M., 2019, "Ethanol Droplet Evaporation: Effects of Ambient Temperature, Pressure and Fuel Vapor Concentration," International Journal of Heat and Mass Transfer, 143, p. 118472.
[4] Renoux, G., 2020, "Étude expérimentale de l'interaction goutte/flamme : Propagation d'une flamme dans un aérosol en microgravité et passage d'une goutte à travers un front de flamme," PhD Thesis, Université d'Orléans.
[5] Thiesset, F., Halter, F., Bariki, C., Lapeyre, C., Chauveau, C., Gökalp, I., Selle, L., and Poinsot, T., 2017, "Isolating Strain and Curvature Effects in Premixed Flame/Vortex Interactions," Journal of Fluid Mechanics, 831, pp. 618–654.
[6] Thielicke, W., and Stamhuis, E. J., 2014, "PIVlab Towards User-Friendly, Affordable and Accurate Digital Particle Image Velocimetry in MATLAB," J. Open Research Software, 2.
[7] Renoux, G., Halter, F., and Chauveau, C., 2018, "Experimental Study of The Morphology of Two-Phase Flame Instabilities in Microgravity," Atomization and Sprays, 28(10), pp. 915–929.
[8] Goodwin, D. G., Speth, R. L., Moffat, H. K., and Weber, B. W., 2018, *Cantera: An Object-Oriented Software Toolkit for Chemical Kinetics, Thermodynamics, and Transport Processes,* Zenodo.
[9] Coffee, T. P., 1984, "Kinetic Mechanisms for Premixed, Laminar, Steady State Methane/Air Flames," Combustion and Flame, 55(2), pp. 161–170.
[10] *Chemical-Kinetic Mechanisms for Combustion Applications*, Mechanical and Aerospace Engineering (Combustion Research), University of California at San Diego.
[11] Moureau, V., Domingo, P., and Vervisch, L., 2011, "Design of a Massively Parallel CFD Code for Complex Geometries," Comptes Rendus Mécanique, 339(2–3), pp. 141–148.
[12] Spalding, D. B., 1950, "Combustion of Liquid Fuels," Nature, 165(4187), pp. 160–160.
[13] Saharin, S. B., Lefort, B., Morin, C., Chauveau, C., Moyne, L. L., and Kafafy, R., 2012, "Vaporization Characteristics of Ethanol And 1-Propanol Droplets at High Temperatures," AAS, 22(3).
[14] Chauveau, C., Birouk, M., Halter, F., and Gokalp, I., 2019, "An Analysis of the Droplet Support Fiber Effect on the Evaporation Process," Int. J. Heat Mass Transf., 128, pp. 885–891.